Supporting Information

Lacroix et al. 10.1073/pnas.1406161111

SI Text

This supplement describes the 2 × 2-state kinetic model including global fit and analysis procedures, model derivation, parameter uncertainty calculations, and procedural details for global fit implementation. Figs. S1–S7 are located below.

Kinetic Modeling

Global Fit and Analysis of the 2 × 2-State Kinetic Model. ***Overview.*** The 2 × 2-state kinetic model was introduced in the main text and Fig. 7*A*, and was constrained by microscopic reversibility (detailed in subsection below). The objective was to fit this model to all experimental data, which consisted of three voltage-dependent curves: τ_A–V, τ_D–V, and Q–V. This was achieved by simultaneously (globally) fitting these data with the respective model-derived functions that describe these curves.

The global fit was initially performed by minimizing the sum of the root-mean-squared errors (RMSEs) for the Q–V and τ–V curve fits. To ensure that each function contributed equally during the minimization, the RMSE were normalized according to the number of experimental points and relative amplitude between Q–V and τ–V data values. Furthermore, we observed that the fit of τ–V curves worsened for voltages far from the sigmoidal region of the corresponding Q–V curves. The reason is that at extreme voltage pulses (far from $V_{1/2}$), gating current kinetics are less voltage-dependent and ultimately become rate-limited by molecular frictions not accounted for in our model (τ are solely limited by V in the model and asymptotically approach $\tau = 0$ ms for $V << V_{1/2}$ or $V >> V_{1/2}$; Fig. 7*C*). To minimize the influence of these points on fit quality, the experimental time constants τ were linearly weighted according to their relative amplitude, thus optimally favoring the voltage-dependent region. To reduce the degrees of freedom in the model, the values of equilibrium constants K_1 and K_2 were initially determined from a global fit of the Q–V and τ–V curves from the WT channel. These values were then used as fixed parameters during the global fit operation for all mutants. Note that we tested and verified that correlation results (Fig. 8) were not affected by even moderate deviations from WT equilibrium constant values.

The quality of each global fit was determined by calculating a quality factor (QF), defined as the mean ratio of global to individual function fit errors. For most mutants, this global fit approach yielded satisfying fits with relatively low QF values ($1 < QF < 6$) (Fig. 7*B*) and relatively small uncertainties for the fitted parameters (i.e., narrow confidence surfaces in Fig. S3). Four mutants yielded QF > 6.5 that were outside the main QF distribution in Fig. 7*B*. These four mutants (I241D, I320Y, F244N, S240F) were considered outliers due to poor global fits (Fig. S4) and were excluded from further analysis. In addition, the mutants A319W and A319N produce activation τ–V curves with unusual "two-bell" shapes (Fig. S5) and were excluded from further analysis.

The remainder of this section derives the 2 × 2-state kinetic model equations and describes the global fit methodology. Subsequent sections describe evaluation of parameter uncertainty and procedural details for the kinetic model fitting used in this study.

Rate equations. The 2 × 2-state kinetic model (Fig. 7*A*) is composed of separate, but circularly connected activation and deactivation pathways. The model rates (α_1, β_1, α_2, β_2, k_{1f}, k_{1b}, k_{2f}, k_{2b}) are linked to the membrane voltage V, absolute temperature T, and Boltzmann constant k by the following rate equations:

$$\alpha_1 = a_{10}\exp\left[z_{1f}V/(kT)\right], \quad \textbf{[S1]}$$

$$\beta_1 = b_{10}\exp\left[-z_{1b}V/(kT)\right], \quad \textbf{[S2]}$$

$$\beta_2 = b_{20}\exp\left[-z_{2b}V/(kT)\right], \quad \textbf{[S3]}$$

$$\alpha_2 = a_{20}\exp\left[z_{2f}V/(kT)\right], \quad \textbf{[S4]}$$

and equilibrium constants: $K_1 = k_{1f}/k_{1b}$ and $K_2 = k_{2f}/k_{2b}$, where f and b represent forward and backward transitions. The set of model parameters consists of the preexponential factors (a_{10}, b_{10}, a_{20}, b_{20}) that define the rate at $V = 0$ mV, the apparent valences (z_{1f}, z_{1b}, z_{2f}, z_{2b}), and K_1 and K_2.

Microscopic reversibility. To ensure microscopic reversibility of the system, the product of all rates in the forward (clockwise) and backward (counterclockwise) directions must be equal. Expressed in terms of α_2, microscopic reversibility constrains the model by Eq. **S5**:

$$\alpha_2 = \frac{\beta_2\alpha_1}{\beta_1}\left(\frac{K_2}{K_1}\right). \quad \textbf{[S5]}$$

Eq. **S5** provides two constraints on the model parameters. First, evaluation of Eq. **S5** at $V = 0$ mV removes voltage dependence, thus yielding a constraint on the preexponential factors. Expressed in terms of a_{20}:

$$a_{20} = \frac{b_{20}a_{10}}{b_{10}}\left(\frac{K_2}{K_1}\right). \quad \textbf{[S6]}$$

Second, division of Eq. **S5** by Eq. **S6** removes the preexponential factors, thus yielding a constraint on the apparent valences. Expressed in terms of z_{2f}:

$$z_{2f} = z_{1f} + z_{1b} - z_{2b}. \quad \textbf{[S7]}$$

These two simplifications reduce the number of independent model parameters from 10 to 8, which is especially important for reliable fit convergence.

Model equations. The charge, activation time constant τ_A, and deactivation time constant τ_D for the 2 × 2-state kinetic model were derived, and are respectively given as follows:

$$\frac{Q}{Q_{max}} = \frac{1+K_2}{1+\frac{\beta_1}{\alpha_1}+K_2\left(1+\frac{\beta_2}{\alpha_2}\right)}, \quad \textbf{[S8]}$$

$$\tau_A = \frac{\alpha_1}{(\alpha_1+\alpha_2)\left[\alpha_1(1+K_2)+\beta_1(1+K_1)\right]} + \frac{\alpha_2}{(\alpha_1+\alpha_2)\left[\alpha_2\left(1+\frac{1}{K_2}\right)+\beta_2\left(1+\frac{1}{K_1}\right)\right]}, \quad \textbf{[S9]}$$

$$\tau_D = \frac{\beta_1(1+K_1)}{(\beta_1+\beta_2)(1+K_2)\left[\alpha_1(1+K_2)+\beta_1(1+K_1)\right]} + \frac{\beta_2\left(1+\frac{1}{K_1}\right)}{(\beta_1+\beta_2)\left(1+\frac{1}{K_2}\right)\left[\alpha_2\left(1+\frac{1}{K_2}\right)+\beta_2\left(1+\frac{1}{K_1}\right)\right]}. \quad \textbf{[S10]}$$

The Q–V voltage midpoint was derived from Eqs. **S1**–**S3**, **S5**, **S8** as follows:

$$V_{1/2}* = \left(\frac{kT}{z_{1f}+z_{1b}}\right)\log\left[\frac{b_{10}}{a_{10}}\left(\frac{1+K_1}{1+K_2}\right)\right]. \quad \textbf{[S11]}$$

Individual function fit. Although underdetermined, we first examined the individual fit of each model function, Eqs. **S8**–**S10**, to its respective data curve. The fit was performed by minimization of the root-mean-square error of the individual weighted objective function:

$$\mathrm{RMSE}_{i,\Omega} = \min_{\boldsymbol{\theta}} \sqrt{\frac{1}{n_\Omega}\sum\left(\xi_\Omega(V)\left[f_\Omega(V;\boldsymbol{\theta}_\Omega)-y_\Omega(V)\right]\right)^2}, \quad \textbf{[S12]}$$

for $\Omega\in\{Q,\tau_A,\tau_D\}$, where $f(V;\boldsymbol{\theta}_\Omega)$ represents the model function defined by the fitted parameter set $\boldsymbol{\theta}_\Omega=(a_{10},b_{10},b_{20},z_{1f},z_{1b},z_{2b})$, and y is the corresponding experimental mean data curve measured at n test voltages V. The least-squares estimate of $\boldsymbol{\theta}_\Omega$ is $\hat{\boldsymbol{\theta}}_\Omega$. Equilibrium constants K_1 and K_2 were fixed to WT values (see text), and thus only six parameters are fit. The Q–V residual weights were uniform: $\xi_\Omega(V)=1$ for $\Omega=Q$; and the τ–V residual weights were linear and normalized: $\xi_\Omega(V)=y(V)/\sum y(V)$ for $\Omega\in\{\tau_A,\tau_D\}$. This linear weighting scheme most accurately fit the upper region of τ–V curves, including the slowest time constant value, while minimizing the influence of the outer/voltage-independent regions that are not well accounted for in our model (lacking a molecular friction term). Due to the overparameterized nature of individually fitting each model function, we found that individual fits for all mutants were remarkably good (within limits of the model).

Global function fit. The 2 × 2-state kinetic model parameters were solved by global analysis, wherein all three model functions, Eqs. **S8**–**S10**, are simultaneously fit to their respective mean data curve (Q–V, τ_A–V, or τ_D–V). This was performed by minimization of the global weighted objective function:

$$\Phi_g = \min_{\boldsymbol{\theta}} \sum_\Omega \omega_\Omega \left\| \xi_\Omega(V)\left[f_\Omega(V;\boldsymbol{\theta})-y_\Omega(V)\right]\right\|_2, \quad \textbf{[S13]}$$

for $\Omega\in\{Q,\tau_A,\tau_D\}$, where double vertical lines denote the L^2-norm, function weights are obtained from individual fits $\omega_\Omega=1/\mathrm{RMSE}_{i,\Omega}$, and the residuals weighting schemes are the same as for individual fits. The least-squares estimate of $\boldsymbol{\theta}$ is $\hat{\boldsymbol{\theta}}$. Once again, equilibrium constants were fixed to WT values, and thus only six parameters are fit. The root-mean-square error of each function from the global fit ($\mathrm{RMSE}_{g,\Omega}$) is calculated by evaluation of Eq. **S12** using the globally derived parameter set $\hat{\boldsymbol{\theta}}$. Importantly, the function weights ω_Ω are required to balance the influence of all three functions. It is possible for an individual function to overfit the data (e.g., too few data points, very low noise), resulting in a disproportionately low RMSE and high influence (weight). To avoid this in the weight calculation, a lower limit was placed on $\mathrm{RMSE}_{i,\Omega}$ corresponding to a fit with error per data point equal to 1% of y_{max} (the typical noise level). We found this method satisfactory for the vast majority of mutants tested. Procedural details for global fitting are discussed in a separate section below.

Goodness of global fit. The goodness of global fit was assessed by the mean ratio of global to individual fit errors, which we refer to as the QF:

$$\mathrm{QF} = \left\langle \frac{\mathrm{RMSE}_{g,\Omega}}{\mathrm{RMSE}_{i,\Omega}} \right\rangle, \quad \textbf{[S14]}$$

for $\Omega\in\{Q,\tau_A,\tau_D\}$. Because the more constrained global fit will always return functions with RMSE higher than an individual fit, the quality factor range is QF ≥ 1, where lower values indicate a better global fit (QF = 1 is optimal). The individual and global fits of all mutants were visually inspected.

Optimization of global function weights. A few mutants (<10%) achieved a visually more balanced fit of model functions by numerical optimization of function weights ω_Ω. In this case, the global fit became a subproblem of a fit to optimize normalized function weights ($\sum\omega_\Omega=1$) by minimization of the QF. The inverse RMSE values were normalized, and used as initial conditions. For consistency and best possible fits, we used this latter method for all mutants.

Parameter Uncertainty and Distribution. Parameter uncertainty was determined by use of the likelihood-ratio criterion. In our case of RMSE-based global fit error, Eq. **S13**, the 100(1 − α)% confidence region (1, 2) of the parameters is given by:

$$\Phi_g(\theta) = \Phi_g(\hat{\theta})\sqrt{\left(1+\frac{p}{n-p}F^\alpha_{p,n-p}\right)}, \quad \textbf{[S15]}$$

where the model has p fitted parameters, $n=\sum n_\Omega$ data observations, and $F^\alpha_{p,n-p}$ is the upper critical value of the $F_{p,n-p}$ distribution at significance level α. To calculate the confidence surface (Fig. S3), the selected parameter is incrementally perturbed to a fixed value away from its optimum (at $\hat{\boldsymbol{\theta}}$), and the model is refit with remaining model parameters variable (3, 4). The global minimum is updated if any improvement is made. Initial conditions are updated to the fit results of the last successful move. This process is repeated until the fit error exceeds the threshold value set by Eq. **S15**. The scan is then repeated in the opposite direction to generate the full confidence surface. The exact confidence interval boundaries are obtained by quadratic interpolation. Here, we developed a "rescue" operation to automatically detect and correct for any spurious (nonsmooth) transitions in each search direction, which can occur if the solver becomes trapped in a local minimum solution. In this case, a refit is performed with all variable parameter initial conditions perturbed by addition of random noise. This process is repeated until an expected improvement (smooth transition) is obtained. After each unsuccessful rescue attempt, the expected improvement criterion is linearly relaxed.

Procedural Details for Kinetic Model Fitting. All data processing and fitting was performed using a custom program developed in the commercial software package MATLAB (The MathWorks). Fits used the built-in constrained optimization solver *fmincon*, with solver parameters and tolerances optimized for our problem. This section discusses important implementation topics.

Parameter transformation. Through examination of fitted parameters from many mutants, we found that the preexponential factors and equilibrium constants (if fitted) were approximately log-normal distributed, whereas the apparent valence terms were in-between log-normal and normally distributed. Therefore, all fitted parameters were log transformed for optimization

by the solver, such that each parameter's base-10 exponent was optimized. Parameters were untransformed during function evaluations. Log transformation of parameters was critical for appropriate sampling and achieving robust convergence to the global minimum solution.

Initial conditions. Because our objective function is nonlinear, initial conditions must be of reasonable quality to ensure convergence to the global minimum solution. The WT dataset was globally fit (with K_1 and K_2 variable) using an exhaustive grid search of different initial parameter combinations to reliably obtain the WT parameter set $\boldsymbol{\theta}^{WT}$: ($K_1 = 1.09e\text{-}5$, $K_2 = 32$, $a_{10} = 0.0398$, $b_{10} = 4.189e\text{-}4$, $b_{20} = 1.295e\text{-}9$, $z_{1f} = 2.4015$, $z_{1b} = 1.7104$, $z_{2b} = 3.4954$), and constrained parameters ($a_{20} = 0.3609$, $z_{2f} = 0.6165$). For all mutant fits, $\boldsymbol{\theta}^{WT}$ was used as parameter initial conditions, and equilibrium constants were held fixed at WT values. Each fit was repeated from different initial conditions until convergence was reached. The initial value for each parameter was randomly sampled according to its known population distribution with mean given by $\boldsymbol{\theta}^{WT}$. Thus, preexponential factors were randomly sampled from a log-normal distribution, and apparent valences were sampled from a normal distribution.

Convergence criterion. To ensure that the global minimum solution was found, each fit was repeated from appropriately randomized initial conditions until a convergence criterion was satisfied ($n =$ 20 solutions must have fit error within 0.1% of the optimum fit error). After convergence, the optimal fit was selected and used for analysis. For the vast majority of mutants tested, ≥95% of sampled fits converged to the optimal solution, thus demonstrating the robustness of the implementation.

Error checking. All fit results were inspected to verify that any/all constraints were satisfied. During function evaluations, precision limits were placed on α and β rate evaluations, Eqs. **S1**–**S5**, to avoid any numerical precision problems (i.e., divide by zero): rate values were bound to the range [1e-30, 1e30].

1. Beale EML (1960) Confidence regions in non-linear estimation. *J R Stat Soc B* 22(1): 41–88.
2. Seber GAF, Wild CJ (1989) *Nonlinear Regression* (Wiley, New York).
3. Hyde HC, et al. (2012) Nano-positioning system for structural analysis of functional homomeric proteins in multiple conformations. *Structure* 20(10):1629–1640.
4. Dalmas O, Hyde HC, Hulse RE, Perozo E (2012) Symmetry-constrained analysis of pulsed double electron-electron resonance (DEER) spectroscopy reveals the dynamic nature of the KcsA activation gate. *J Am Chem Soc* 134(39):16360–16369.

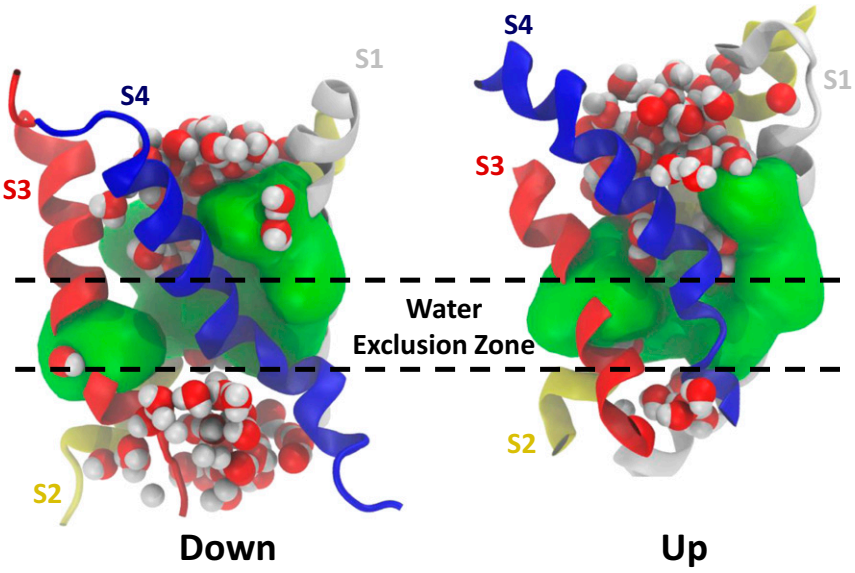

Fig. S1. Conservation of gating pore function in different voltage sensor domain (VSD) conformations. The figure depicts structural models of the Kv1.2 channel VSD with explicit solvent and lipid molecules (from ref. 1) in hyperpolarized ("Down"; *Left*) and depolarized ("Up"; *Right*) states. The VSD helices are colored as follows: S1, white; S2, yellow; S3, red; and S4, blue. The green surface represents the van der Waals surface of the 10 gating pore residues analyzed in this study (V236, I237, S240, I241, F244, C286, I287, F290, A319, and I320 in Shaker numbering), and the water molecules are represented by red and white spheres. Note that, in both states, the gating pore delineates a water exclusion zone (black dotted lines).

1. Khalili-Araghi F, et al. (2010) Calculation of the gating charge for the Kv1.2 voltage-activated potassium channel. *Biophys J* 98(10):2189–2198.

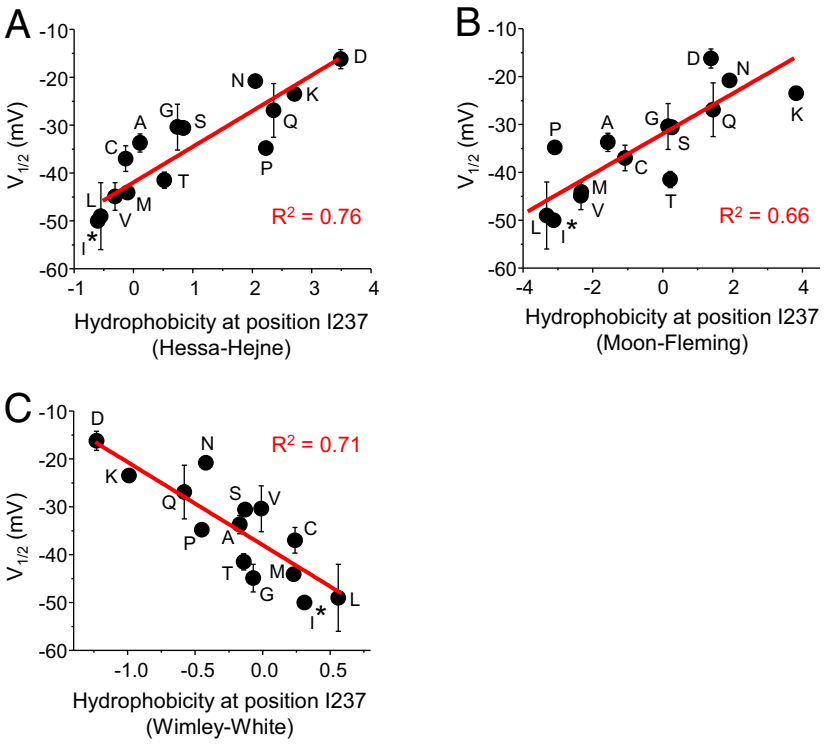

Fig. S2. Additional relations between gating charge movement and hydrophobicity of substituted amino acids at position I237. (*A*–*C*) The mean $V_{1/2}$ values obtained from each *Q*–*V* curve of Fig. 3*A* are plotted as a function of the hydrophobicity of the substituted side chain at position I237, using three additional hydrophobicity scales: (*A*) Hessa–Hejne, (*B*) Moon–Fleming, and (*C*) Wimley–White. The R^2 values indicate the goodness of a linear fit to the data (red lines), and letters indicate the substituted amino acid. The asterisk (*) indicates the native amino acid.

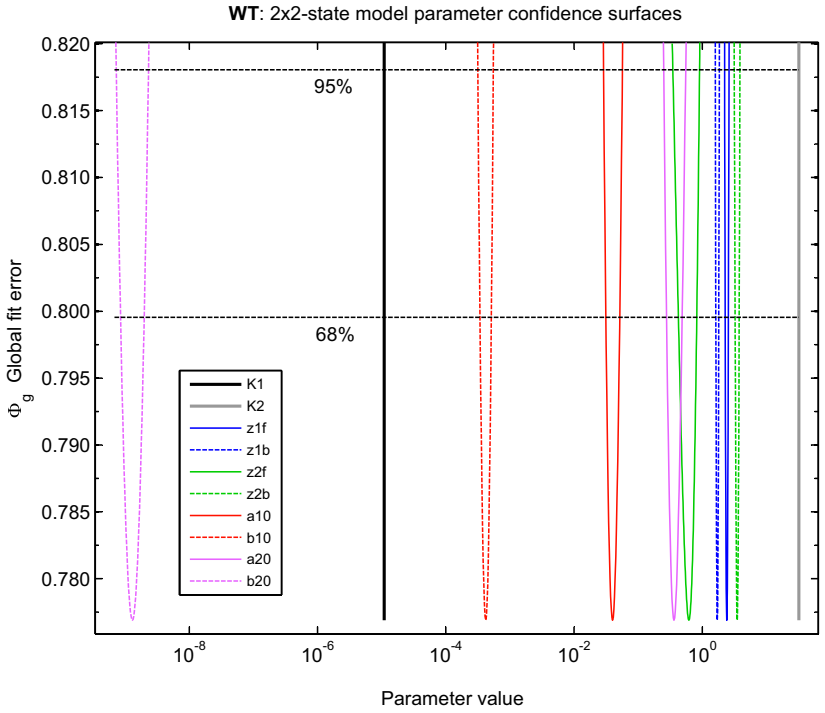

Fig. S3. Confidence surfaces for globally fitted parameters from WT Shaker. For a nonlinear model, the uncertainty in parameter estimation is most accurately given by rigorous calculation of the exact confidence surface, as shown here for WT Shaker. Briefly, the method is to fit the model with one parameter incrementally perturbed (fixed) away from its optimal value until the fit error exceeds the desired statistical threshold. The procedure is then repeated in the opposite direction. The dotted lines represent the 1σ (68%) and 2σ (95%) confidence levels. Equilibrium constants K_1 and K_2 are displayed as vertical lines at their fixed values. This figure demonstrates that all parameters of our 2 × 2-state kinetic model are well determined when K_1 and K_2 are fixed (or even moderately constrained, not shown here).

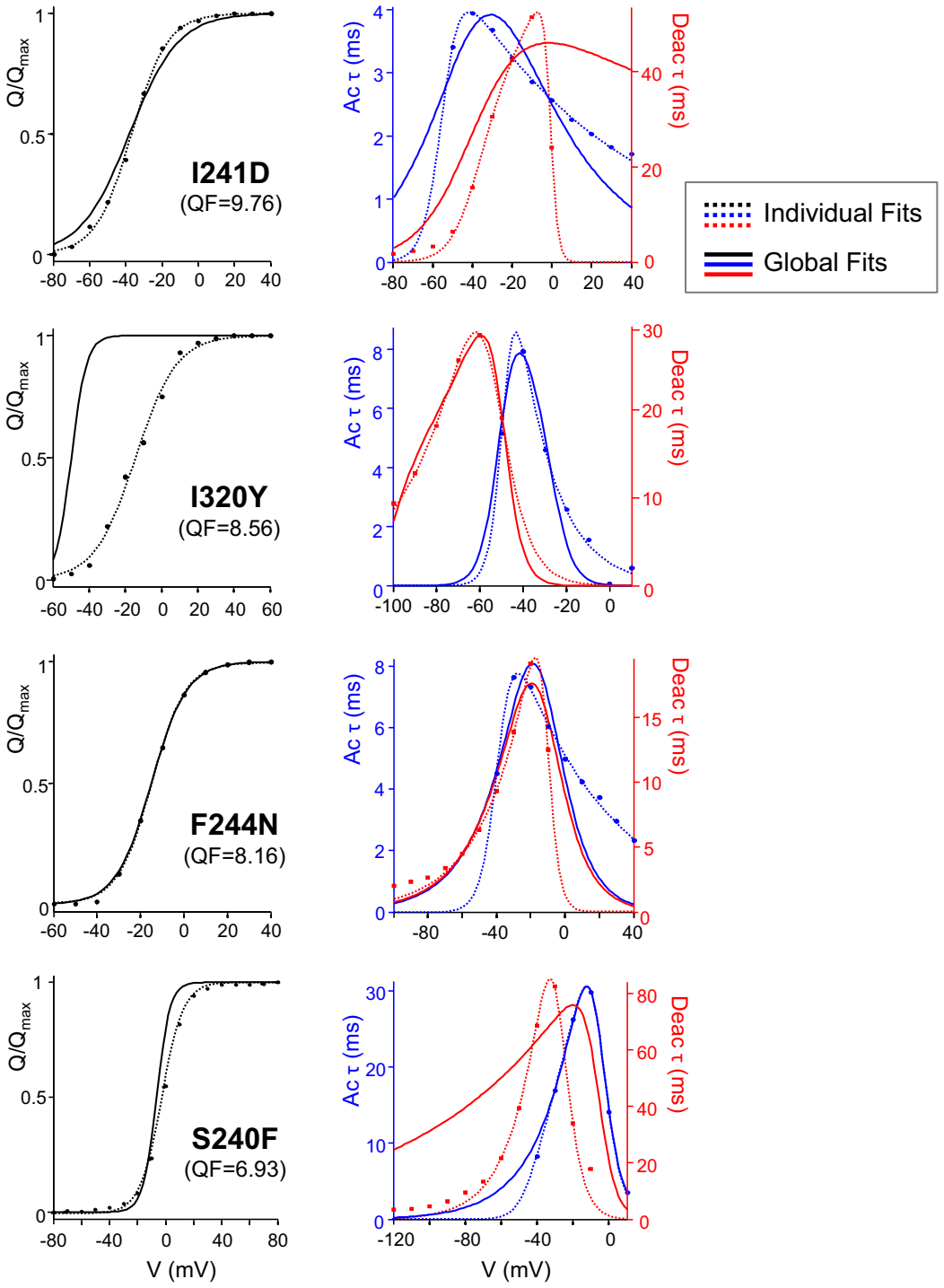

Fig. S4. Gating pore mutations leading to poor global fits. The figure shows the individual (dotted lines) and global (solid lines) fits and data points for the gating functions (*Q–V*, black; activation τ–*V*, blue; and deactivation τ–*V*, red) of the I241D, I320Y, F244N, and S240F mutants, which produce poor global fits (QF > 6.5; see parentheses). The I241D mutation leads to poor global fits of the three gating functions (*Q–V* and τ–*V* curves). The global fit for the mutant I320Y and S240F led to a poor fit of the *Q–V* curve and deactivation τ–*V* curve, respectively. The poor QF value obtained for the F244N mutant is mainly due to the exceptionally good individual fits of its gating functions.

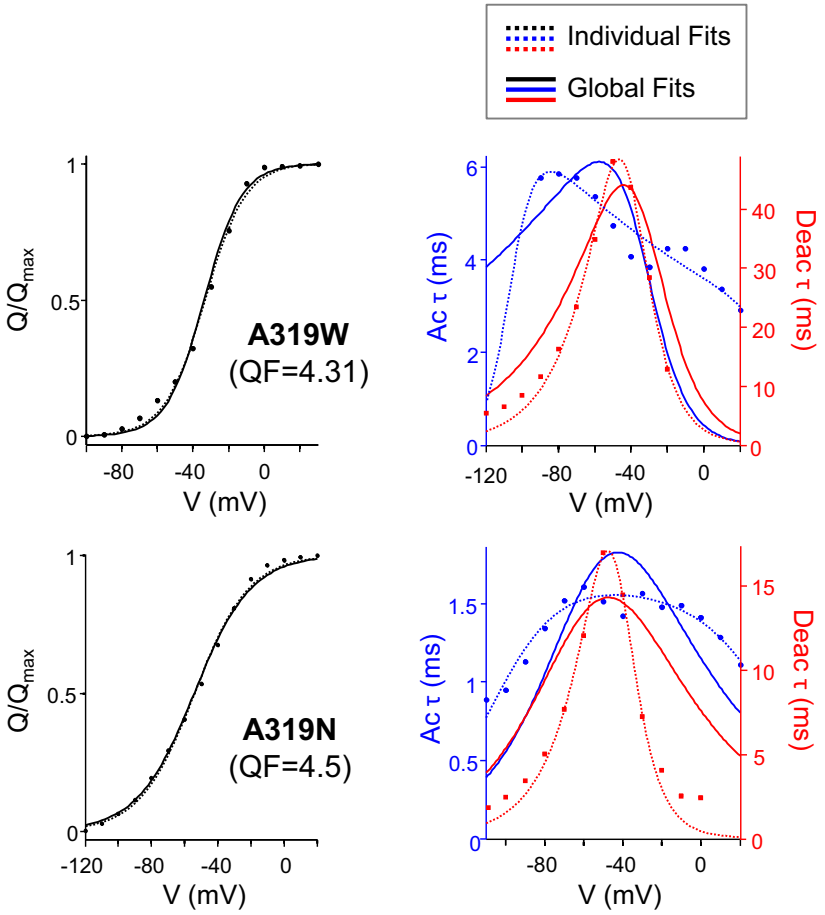

Fig. S5. The A319W and A319N mutations produce activation τ–V curves with an atypical two-bell shape. The figure shows the individual (dotted lines) and global (solid lines) fits and data points for the gating functions (Q–V, black; activation τ–V, blue; and deactivation τ–V, red) of the A319W and A319N mutants. Note the atypical two-bell shape of the activation τ–V plots, which led to poor fits.

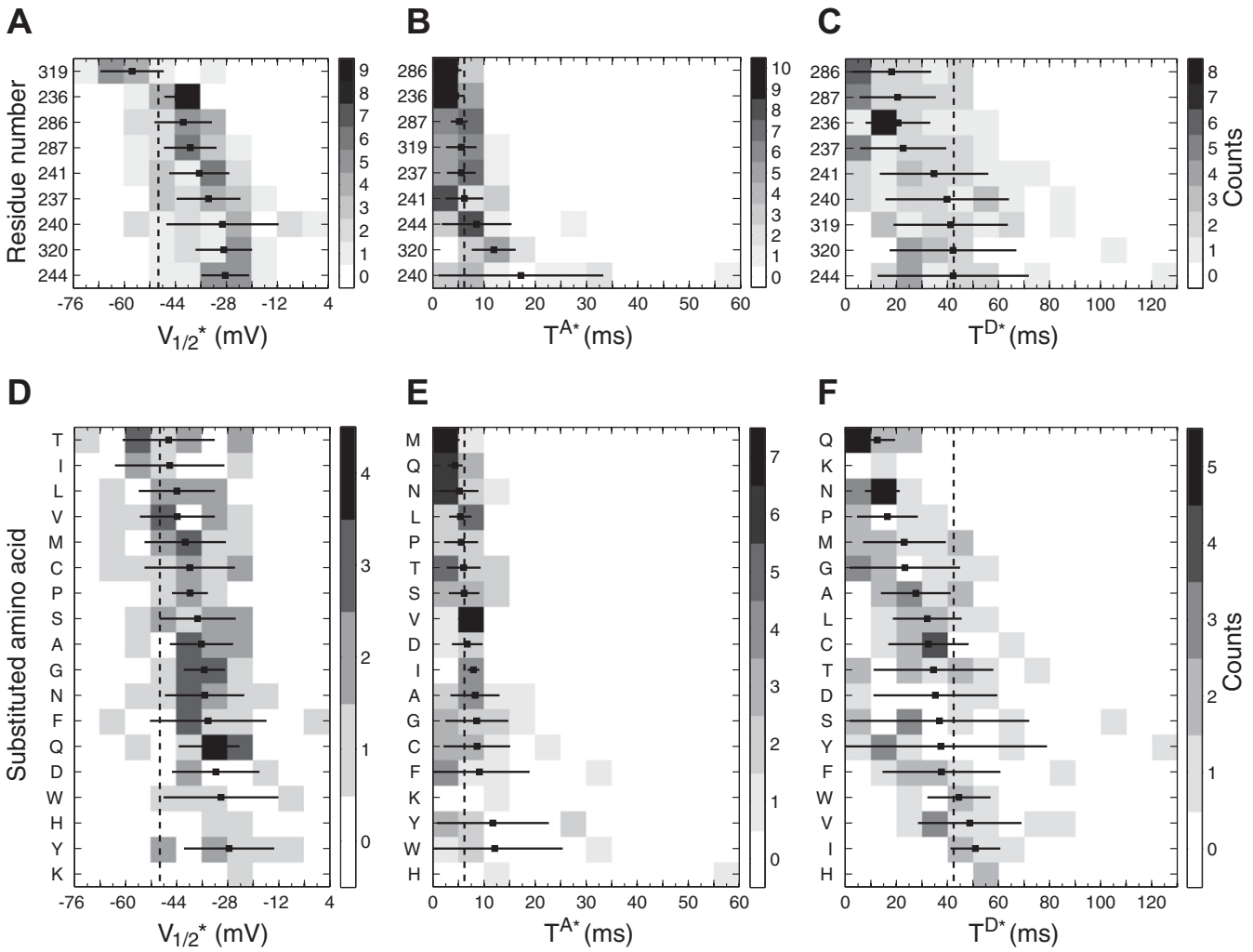

Fig. S6. Global effects of gating pore mutations on observable gating parameters. (*A*–*F*) The distribution of mutational phenotypes are shown as a function of the mutated position (*Upper*) or as a function of the substituted amino acid (*Lower*) for observable gating parameters $V_{1/2}$* (*A* and *D*), T^{A}* (*B* and *E*), and T^{D}* (*C* and *F*). In each panel, the marker/line pair represents the mean and SD per row, the rows are sorted by mean value, and the vertical dashed line represents the WT value. The observable gating parameters shown are high-resolution values derived from the model fit of individual functions. Note that most mutations displace the *Q*–*V* curve $V_{1/2}$* toward more positive voltages and accelerate deactivation (smaller T^{D} values).

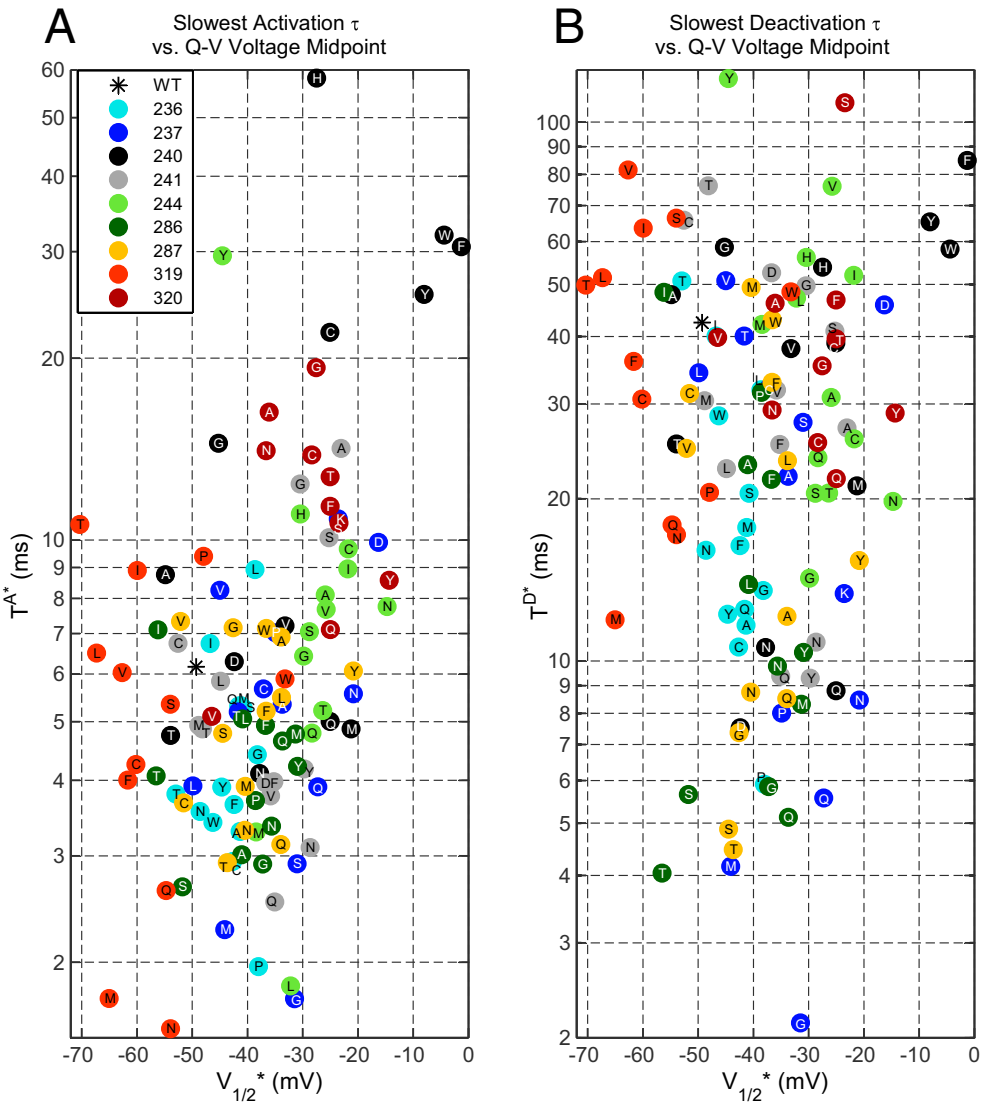

Fig. S7. The side chain of gating pore residues modulates gating kinetics and the *Q–V* voltage midpoint over a large dynamic range. (*A*) Relation between slowest activation time constant and *Q–V* voltage midpoint. (*B*) Relation between slowest deactivation time constant and *Q–V* voltage midpoint. All gating pore mutants fit by the 2 × 2-state kinetic model are displayed (except 286V, which overlaps WT). The observable gating parameters shown are high-resolution values derived from the model fit of individual functions. Note that the goodness of fit for individual functions was excellent for all mutants shown here.